Supporting Information

An et al. 10.1073/pnas.1307088110

SI Text

A Computational Model of Circadian Desynchronization Predicts Faster Entrainment

How can vasoactive intestinal polypeptide (VIP) both synchronize and desynchronize circadian cells? Underlying this apparent contradiction may be a phase-tumbling mechanism similar to the "run and tumble" mechanism of bacterial chemotaxis (1), where suprachiasmatic nucleus (SCN) neurons receiving VIP stimulation at a phase far from the phase angle of entrainment would "tumble" their phases. This would result in reduced synchrony among the circadian cells. In contrast, SCN neurons receiving VIP stimulation near their phase angle of entrainment would "run" toward it.

A fundamental consequence of the phase-tumbling hypothesis is that a desynchronized SCN should entrain faster than a synchronized SCN to a large shift in the environmental cycle. To test this, we generated a cell model that is a stochastic adaptation of Leloup and Goldbeter's deterministic model of circadian gene regulation (2) that includes coupling (3) and a mechanism for light input (4). In our simulations, cells were initialized with either random or synchronized phases. The light cycle was simulated with daily release of VIP. The phases of the cells were tracked by the time of their daily Period (PER) protein peak, using the Morlet continuous wavelet transform (5). Our stochastic model of the SCN predicted that cells with random initial phases would entrain, on average, 1–5 d faster (depending on the size of the scheduled shift) than cells with synchronized phases. Further, it predicted that VIP exposure would reduce the amplitude of the synchronized population by reducing synchrony (Fig. S2). Thus, importantly, the stochastic model can explain both the desynchronization and rapid entrainment of the SCN by VIP.

The phase-tumbling hypothesis was motivated by the phase response distribution (PRD) (Fig. S3) of our stochastic model. A PRD is similar to a phase response curve (PRC), in that it plots the change of phase as the result of a pulse of light (represented in our model as a pulse of VIP) at a given time. It differs from the PRC in that it shows the distribution of the responses, as opposed to the aggregate response. There are a number of important features of this PRD. First, note that the region that is roughly between circadian time (CT)2 and CT10 is stable, in the sense that a pulse of light is unlikely to shift the phase outside this region and is in fact likely to shift the phase toward the phase angle of entrainment near CT4. Second, there is greater phase dispersion outside this region, with greatest phase dispersion occurring near CT22. In short, given a pulse of light between CT2 and CT10, the circadian cells are running toward CT4 (but occasionally tumbling along the way). In contrast, given a pulse of light elsewhere, the cells are more likely to be tumbling their phases.

To see the effects of desynchronization using the PRD, consider starting with a synchronized system and applying a pulse of light at CT19.5 and every 24 h thereafter. The full distribution information available in the PRD is used to determine the probability that a cell at a given CT will shift to any other CT. To do this, we bin the CTs and form a histogram, as shown in Fig. S3, and then we apply the entrainment signal. Fig. S3, *Left* shows the phase distribution at 24-h intervals for cells that are completely desynchronized when they receive the initial entrainment signal. Fig. S3, *Right* illustrates the process of entrainment to a large shift in the environmental cycle for cells that are initially synchronized: It is clear that the cells first desynchronize and then entrain; hence the total time to entrainment is longer than if they had started out desynchronized.

Intrinsic stochasticity, due to small populations of key chemical species, naturally results in a PRD that is consistent with phase tumbling. The structure of the Leloup and Goldbeter (2) model suggests the source of the variability in the phase dispersion. The rate of change of Per mRNA in the nucleus is defined as the sum of three terms that characterize (*i*) the transcription rate, (*ii*) the transport rate from the nucleus to the cytoplasm, and (*iii*) the Per mRNA degradation rate. Augmenting VIP increases the variability of nuclear Per mRNA accumulation when nuclear–cytoplasmic transport rates and degradation rates are low (near CT22), whereas the effect of VIP application near CT4, when transport and degradation rates are high, is much smaller.

Model Description

The behavior of circadian cells in the SCN was modeled with a 2D 7×7 rectangular grid of 49 stochastic circadian cells. Each cell was coupled to its two nearest surrounding neighbors (5×5 kernel) via intercellular VIP signaling (3). Periodic (wrap) boundary conditions were used at the edge of the overall 7×7 grid. Each stochastic cell is defined by a set of discrete stochastic reactions (Tables S1–S3) that represent its internal gene regulatory network. We adapted the Leloup and Goldbeter 16-state deterministic model (2) to a discrete stochastic model by using a scaling constant $\Omega = 90$ to convert molar concentrations to number of molecules (4). All parameter values (Table S4) were the same as reported by Leloup and Goldbeter (2) and To et al. (3) except the basal Per mRNA transcription rate ($\nu_{sP0} = 1.1$) and maximum effect of the CREB-binding element on the Per gene ($C_T = 0.4$).

The addition of VIP was modeled by increasing the Per transcription rate to $\nu_{sP0} = 5.5$ and then decaying exponentially back to 1.1 with a half-life and duration of 2 h. Initial conditions were chosen from the result of a previous synchronized (unperturbed) run at either different random times for each cell (for a desynchronized initial condition) or a single time for all cells (for a synchronized initial condition). Simulations were performed using the direct method of the stochastic simulation algorithm (SSA) (6). Time steps ranged from 2e-13 h to 2e-4 h and results were recorded at time intervals of 0.1 h. The simulation was coded in the C++ programming language and run on the Triton Compute Cluster at the San Diego Supercomputer Center.

To convert molar concentrations in the deterministic model to populations (number of each chemical species) requires converting the concentration to units of molecules per liter and then multiplying by a cell volume V. The scaling constant Ω is given by

$$\Omega = N_A\,[\text{molecules/liter}] \times V\,[\text{liters}], \qquad \textbf{[S1]}$$

where Avogadro's number $N_A = 6.022 \times 10^{23}$.

Intercellular Coupling

The intercellular coupling (3) is defined by the following equations. The VIP produced by a cell is

$$\rho_i(t) = a\Omega \frac{M_{P,i}(t)}{M_{P,i}(t) + b\Omega}. \qquad \textbf{[S2]}$$

The VIP observed by cell i due to cell j is

$$\gamma_i(t) = \frac{1}{\epsilon} \sum_{j=1}^{N} \alpha_{ij} \rho_j(t), \qquad \textbf{[S3]}$$

where α_{ij} is the reciprocal of the distance between cells i and j.

The sum of weight factors across the population is

$$\epsilon = \frac{1}{N}\sum_{i=1}^{N}\sum_{j=1}^{N}\alpha_{ij}. \quad [S4]$$

The receptor density is

$$\beta = \frac{\gamma}{K_D\Omega + \gamma}. \quad [S5]$$

The cytosolic calcium balance is

$$k\Omega Ca^{2+}_{Cytosol} = \nu_0\Omega + \nu_1\Omega\beta. \quad [S6]$$

The maximum kinase rate is

$$\nu_K = V_{M\,K}\Omega\frac{Ca^{2+}_{Cytosol}}{K_a + Ca^{2+}_{Cytosol}}. \quad [S7]$$

The extent of CREB activation is

$$\lambda = \frac{CB_T CB^*}{K_C\Omega + CB_T CB^*}. \quad [S8]$$

The maximum per transcription rate is

$$\nu_{sP} = \nu_{sP0}\Omega + C_T\lambda. \quad [S9]$$

Data Analysis

Simulation data were analyzed using the Morlet continuous wavelet transform (CWT) as follows: To reduce edge effects, the original data for analysis were first mean centered and then padded with equal-length zeros at the beginning and end of the dataset. The CWT was calculated in the Fourier domain, using published methods (7), after which the zero padding was removed. The standard representation of scales as voices within octaves was used, with 32 voices per octave. The translation-by-translation maximum of the norm was selected as the ridge, from which the instantaneous period and phase were obtained (8). Synchronization was evaluated from phase vectors via the Rayleigh statistic (9) as the magnitude of the mean phase vector across all cells; this value ranges between 0 and 1, where a value of 1 indicates perfect synchronization with all oscillators at identical phases, and a value of 0 indicates a uniform distribution of phases about the clock. All wavelet transforms were performed in MATLAB, using the WAVOS wavelet analysis package, which is freely available for download from http://sourceforge.net/projects/wavos/files/.

1. Berg HC, Brown DA (1972) Chemotaxis in Escherichia coli analysed by three-dimensional tracking. *Nature* 239(5374):500–504.
2. Leloup JC, Goldbeter A (2003) Toward a detailed computational model for the mammalian circadian clock. *Proc Natl Acad Sci USA* 100(12):7051–7056.
3. To TL, Henson MA, Herzog ED, Doyle FJ III (2007) A molecular model for intercellular synchronization in the mammalian circadian clock. *Biophys J* 92(11):3792–3803.
4. Bagheri N, Taylor SR, Meeker K, Petzold LR, Doyle FJ III (2008) Synchrony and entrainment properties of robust circadian oscillators. *J R Soc Interface* 5(0, Suppl 1): S17–S28.
5. Harang R, Bonnet G, Petzold LR (2012) WAVOS: A MATLAB toolkit for wavelet analysis and visualization of oscillatory systems. *BMC Res Notes* 5(1):163.
6. Gillespie DT (1976) A general method for numerically simulating the stochastic time evolution of coupled chemical reactions. *J Comput Phys* 22:403–434.
7. Torrence C, Compo GP (1998) A practical guide to wavelet analysis. *Bull Am Meteorol Soc* 79:6178.
8. Mallat S (1999) *A Wavelet Tour of Signal Processing* (Academic, London).
9. Batschelet E, Sibson R, Cohen JE (1981) *Circular Statistics in Biology*, Mathematics in Biology (Academic, New York).

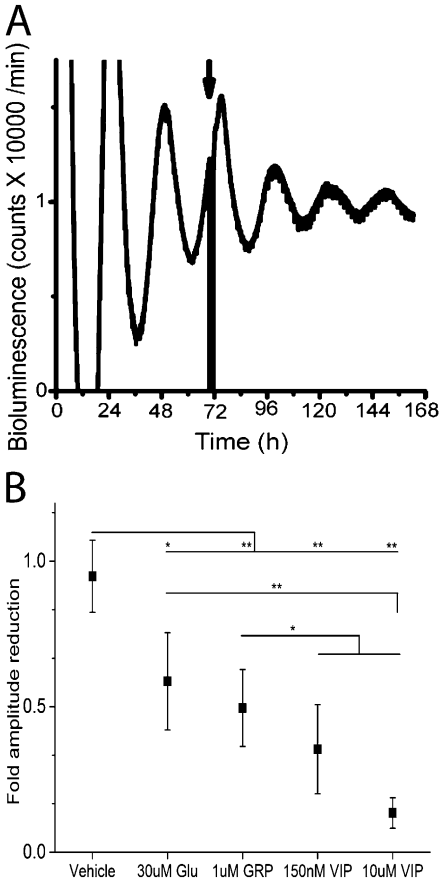

Fig. S1. (*A*) VIP reduces the amplitude of PER2 rhythms after three washes. A representative trace from a SCN explant treated with 10 μM VIP at CT11 (arrow), followed by three full medium changes after 1 h, shows that the amplitude of PER2 rhythms decreased rapidly and slowly recovered similar to that in cultures treated without removing VIP from the dish. (*B*) Compared with VIP, stimulation with 30 μM glutamate (Glu) or 1 μM gastrin-releasing peptide (GRP) at CT22 modestly reduced the amplitude of PER2 expression on the day after application (*$P < 0.05$, **$P < 0.01$; one-way ANOVA followed by a Scheffé test; $n = 4–7$ SCN per treatment).

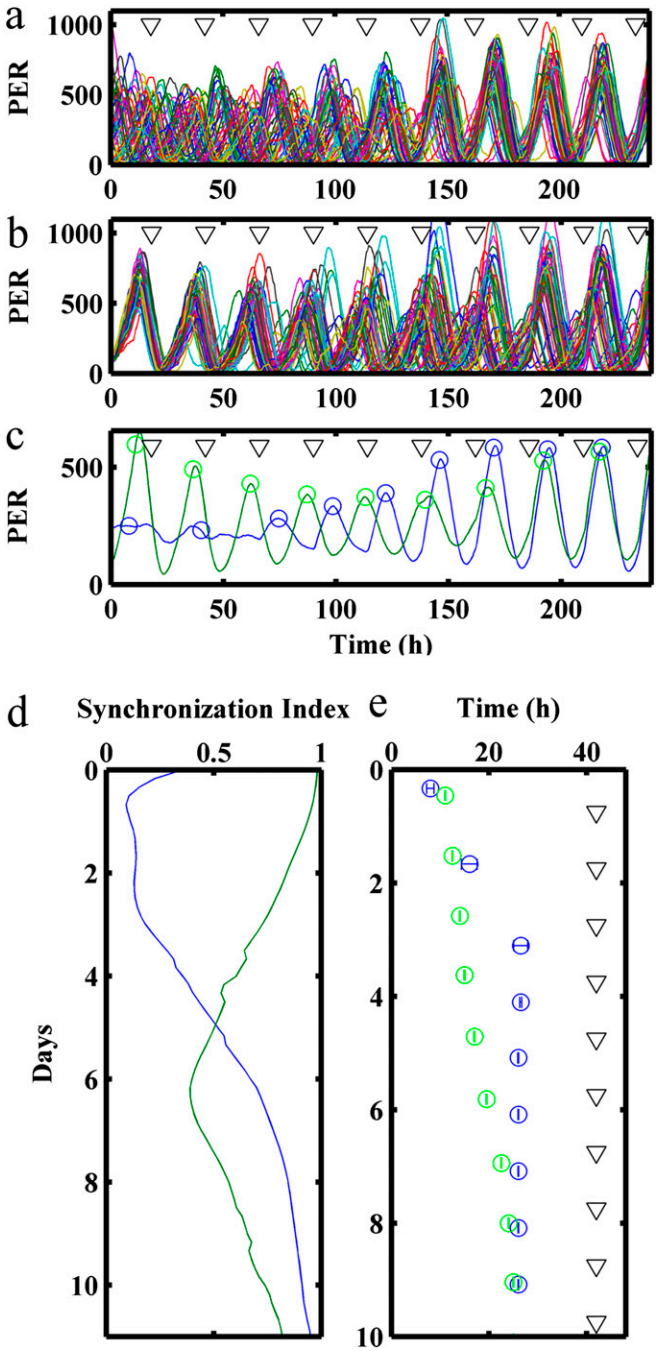

Fig. S2. A computational model reveals that phase tumbling of circadian oscillators explains VIP-induced desynchrony and predicts that phase tumbling can speed entrainment. (*A* and *B*) PER protein levels from stochastic simulations of 49 SCN neurons started with (*A*) random and (*B*) synchronized initial phases and then were subjected to a 10-h phase shift via VIP pulses every 24 h (triangles). (*C*) The mean mRNA level of the 49 cells illustrates the loss of amplitude in the population signal due to loss of synchrony between cells that were initially synchronized (green) or desynchronized (blue). Circles mark PER peaks. (*D*) Synchronization index and (*E*) daily peaks of PER (circles, mean ± SEM) show that desychronized cells (blue) entrain to VIP (triangles) more quickly than synchronized cells (green).

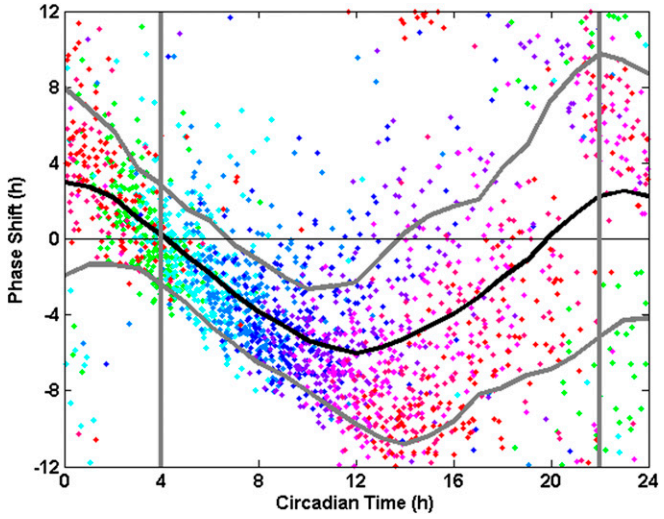

Fig. S3. Model SCN cells display a time-dependent, stochastic response to VIP stimulation. Consistent with the published phase response curve to VIP, on average (black line), VIP delayed circadian rhythms of individual cells when applied during most of the subjective day (CT5–20) and advanced rhythms when applied during the late subjective night to early morning (CT20–5). The SD of the phase shifts (gray lines) was greatest around CT22 and smallest around CT4 (vertical gray lines). Each point represents the shift of a single, simulated cell in a single VIP application. Each color shows results from five repeated, Monte Carlo trials simulating VIP treatment of 49 uncoupled cells. CT0 was defined as the minimum in *Period* gene expression as determined by WAVOS, a MATLAB toolkit for wavelet analysis (5). Note that the time of least-phase dispersion (CT4) corresponds to the published time when daily VIP entrains SCN rhythms, but that VIP at any time induces phase dispersion (tumbling). These computational modeling results provide a mechanism by which VIP both reduces synchrony among cells and, when released daily, can entrain SCN rhythms.

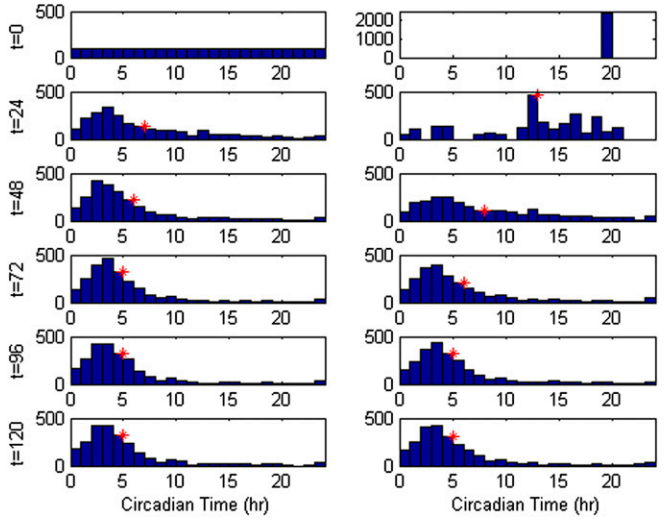

Fig. S4. A pulse of light was applied to the simulated cells at CT19.5 and every 24 h thereafter. Histograms showing the distribution of cells at 24-h intervals were computed from the PRD. They show rapid convergence to the stable point near CT4 when the initial distribution is desynchronized (*Left*). When the initial distribution is synchronized (*Right*), the cells first desynchronize before reentraining and converging to the stable point near CT4. The red asterisks show the mean time of maximal PER expression of each distribution of simulated cells.

Table S1. Reactions in 16-state Leloup and Goldbeter model

Reaction no.	Reaction	Probability of reaction	Transition
$\frac{dM_P}{dt}$			
0	$G \rightarrow G + M_P$	$w_0 = (\nu_{sP}\Omega)\frac{B_N^n}{(K_{AP}\Omega)^n + B_N^n}$	$M_P \rightarrow M_P + 1$
1	$M_P \rightarrow$	$w_1 = (\nu_{mP}\Omega)\frac{M_P}{(K_{mP}\Omega) + M_P}$	$M_P \rightarrow M_P - 1$
2	$M_P \rightarrow$	$w_2 = k_{dmp}M_P$	$M_P \rightarrow M_P - 1$
$\frac{dM_C}{dt}$			
3	$G \rightarrow G + M_C$	$w_3 = (\nu_{sC}\Omega)\frac{B_N^n}{(K_{AC}\Omega)^n + B_N^n}$	$M_C \rightarrow M_C + 1$
4	$M_C \rightarrow$	$w_4 = (\nu_{mC}\Omega)\frac{M_C}{(K_{mC}\Omega) + M_C}$	$M_C \rightarrow M_C - 1$
5	$M_C \rightarrow$	$w_5 = k_{dmc}M_C$	$M_C \rightarrow M_C - 1$
$\frac{dM_B}{dt}$			
6	$G \rightarrow G + M_B$	$w_6 = (\nu_{sB}\Omega)\frac{(K_{IB}\Omega)^m}{(K_{IB}\Omega)^m + B_N^m}$	$M_B \rightarrow M_B + 1$
7	$M_B \rightarrow$	$w_7 = (\nu_{mb}\Omega)\frac{M_B}{(K_{mB}\Omega) + M_B}$	$M_B \rightarrow M_B - 1$
8	$M_B \rightarrow$	$w_8 = k_{dmb}M_B$	$M_B \rightarrow M_B - 1$
$\frac{dP_C}{dt}$			
9	$M_P \rightarrow P_C$	$w_9 = k_{sp}M_P$	$P_C \rightarrow P_C + 1$
10	$P_C \rightarrow P_{CP}$	$w_{10} = (V_{1P}\Omega)\frac{P_C}{(K_p\Omega) + P_C}$	$P_C \rightarrow P_C - 1$
11	$P_{CP} \rightarrow P_C$	$w_{11} = (V_{2P}\Omega)\frac{P_{CP}}{(K_{dp}\Omega) + P_{CP}}$	$P_{CP} \rightarrow P_{CP} + 1$ $P_C \rightarrow P_C + 1$
12	$PC_C \rightarrow P_C + C_C$	$w_{12} = k_4 PC_C$	$P_{CP} \rightarrow P_{CP} - 1$ $P_C \rightarrow P_C + 1$
13	$P_C + C_C \rightarrow PC_C$	$w_{13} = \left(\frac{k_3}{\Omega}\right)P_C C_C$	$C_C \rightarrow C_C + 1$ $PC_C \rightarrow PC_C - 1$ $P_C \rightarrow P_C - 1$
14	$P_C \rightarrow$	$w_{14} = k_{dn}P_C$	$C_C \rightarrow C_C - 1$ $PC_C \rightarrow PC_C + 1$ $P_C \rightarrow P_C - 1$
$\frac{dC_C}{dt}$			
15	$M_C \rightarrow C_C$	$w_{15} = k_{sC}M_C$	$C_C \rightarrow C_C + 1$
16	$C_C \rightarrow C_{CP}$	$w_{16} = (V_{1C}\Omega)\frac{C_C}{(K_p\Omega) + C_C}$	$C_C \rightarrow C_C - 1$
17	$C_{CP} \rightarrow C_C$	$w_{17} = (V_{2C}\Omega)\frac{C_{CP}}{(K_{dp}\Omega) + C_{CP}}$	$C_{CP} \rightarrow C_{CP} + 1$ $C_C \rightarrow C_C + 1$
18	$C_C \rightarrow$	$w_{18} = k_{dnc}C_C$	$C_{CP} \rightarrow C_{CP} - 1$ $C_C \rightarrow C_C - 1$
$\frac{dP_{CP}}{dt}$			
19	$P_{CP} \rightarrow$	$w_{19} = (\nu_{dPC}\Omega)\frac{P_{CP}}{(K_d\Omega) + P_{CP}}$	$P_{CP} \rightarrow P_{CP} - 1$
20	$P_{CP} \rightarrow$	$w_{20} = k_{dn}P_{CP}$	$P_{CP} \rightarrow P_{CP} - 1$
$\frac{dC_{CP}}{dt}$			
21	$C_{CP} \rightarrow$	$w_{21} = (\nu_{dCC}\Omega)\frac{C_{CP}}{(K_d\Omega) + C_{CP}}$	$C_{CP} \rightarrow C_{CP} - 1$
22	$C_{CP} \rightarrow$	$w_{22} = k_{dn}C_{CP}$	$C_{CP} \rightarrow C_{CP} - 1$

Table S2. Reactions in 16-state Leloup and Goldbeter model

Reaction no.	Reaction	Probability of reaction	Transition
$\frac{dPC_C}{dt}$			
23	$PC_C \rightarrow PC_{CP}$	$w_{23} = (V_{1PC}\Omega)\frac{PC_C}{(K_p\Omega) + PC_C}$	$PC_C \rightarrow PC_C - 1$
24	$PC_{CP} \rightarrow PC_C$	$w_{24} = (V_{2PC}\Omega)\frac{PC_{CP}}{(K_{dp}\Omega) + PC_{CP}}$	$PC_{CP} \rightarrow PC_{CP} + 1$ $PC_C \rightarrow PC_C + 1$
25	$PC_N \rightarrow PC_C$	$w_{25} = k_2 PC_N$	$PC_{CP} \rightarrow PC_{CP} - 1$ $PC_C \rightarrow PC_C + 1$
26	$PC_C \rightarrow PC_N$	$w_{26} = k_1 PC_C$	$PC_N \rightarrow PC_N - 1$ $PC_C \rightarrow PC_C - 1$
27	$PC_C \rightarrow$	$w_{27} = k_{dn} PC_C$	$PC_N \rightarrow PC_N + 1$ $PC_C \rightarrow PC_C - 1$
$\frac{dPC_N}{dt}$			
28	$PC_N \rightarrow PC_{NP}$	$w_{28} = (V_{3PC}\Omega)\frac{PC_N}{(K_p\Omega) + PC_N}$	$PC_N \rightarrow PC_N - 1$
29	$PC_{NP} \rightarrow PC_N$	$w_{29} = (V_{4PC}\Omega)\frac{PC_{NP}}{(K_{dp}\Omega) + PC_{NP}}$	$PC_{NP} \rightarrow PC_{NP} + 1$ $PC_N \rightarrow PC_N + 1$
30	$PC_N + B_N \rightarrow I_N$	$w_{30} = \left(\frac{k_7}{\Omega}\right) PC_N B_N$	$PC_{NP} \rightarrow PC_{NP} - 1$ $PC_N \rightarrow PC_N - 1$
31	$I_N \rightarrow PC_N + B_N$	$w_{31} = k_8 I_N$	$B_N \rightarrow B_N - 1$ $I_N \rightarrow I_N + 1$
32	$PC_N \rightarrow$	$w_{32} = k_{dn} PC_N$	$PC_N \rightarrow PC_N + 1$ $B_N \rightarrow B_N + 1$ $I_N \rightarrow I_N - 1$ $PC_N \rightarrow PC_N - 1$
$\frac{dPC_{CP}}{dt}$			
33	$PC_{CP} \rightarrow$	$w_{33} = (V_{dPCC}\Omega)\frac{PC_{CP}}{(K_d\Omega) + PC_{CP}}$	$PC_{CP} \rightarrow PC_{CP} - 1$
34	$PC_{CP} \rightarrow$	$w_{34} = k_{dn} PC_{CP}$	$PC_{CP} \rightarrow PC_{CP} - 1$
$\frac{dPC_{NP}}{dt}$			
35	$PC_{NP} \rightarrow$	$w_{35} = (V_{dPCN}\Omega)\frac{PC_{NP}}{(K_d\Omega) + PC_{NP}}$	$PC_{NP} \rightarrow PC_{NP} - 1$
36	$PC_{NP} \rightarrow$	$w_{36} = k_{dn} PC_{NP}$	$PC_{NP} \rightarrow PC_{NP} - 1$
$\frac{dB_C}{dt}$			
37	$M_B \rightarrow B_C$	$w_{37} = k_{sB} M_B$	$B_C \rightarrow B_C + 1$
38	$B_C \rightarrow B_{CP}$	$w_{38} = (V_{1B}\Omega)\frac{B_C}{(K_p\Omega) + B_C}$	$B_C \rightarrow B_C - 1$
39	$B_{CP} \rightarrow B_C$	$w_{39} = (V_{2B}\Omega)\frac{B_{CP}}{(K_{dp}\Omega) + B_{CP}}$	$B_{CP} \rightarrow B_{CP} + 1$ $B_C \rightarrow B_C + 1$
40	$B_C \rightarrow B_N$	$w_{40} = k_5 B_C$	$B_{CP} \rightarrow B_{CP} - 1$ $B_C \rightarrow B_C - 1$
41	$B_N \rightarrow B_C$	$w_{41} = k_6 B_N$	$B_N \rightarrow B_N + 1$ $B_C \rightarrow B_C + 1$
42	$B_C \rightarrow$	$w_{42} = k_{dn} B_C$	$B_N \rightarrow B_N - 1$ $B_C \rightarrow B_C - 1$
$\frac{dB_{CP}}{dt}$			
43	$B_{CP} \rightarrow$	$w_{43} = (V_{dBC}\Omega)\frac{B_{CP}}{(K_d\Omega) + B_{CP}}$	$B_{CP} \rightarrow B_{CP} - 1$
44	$B_{CP} \rightarrow$	$w_{44} = k_{dn} B_{CP}$	$B_{CP} \rightarrow B_{CP} - 1$

Table S3. Reactions in 17-state model based on 16-state Leloup and Goldbeter model with added CREB equation

Reaction no.	Reaction	Probability of reaction	Transition
$\frac{dB_N}{dt}$			
45	$B_N \rightarrow B_{NP}$	$w_{45} = (V_{3B}\Omega)\frac{B_N}{(K_p\Omega) + B_N}$	$B_N \rightarrow B_N - 1$
46	$B_{NP} \rightarrow B_N$	$w_{46} = (V_{4B}\Omega)\frac{B_{NP}}{(K_{dp}\Omega) + B_{NP}}$	$B_{NP} \rightarrow B_{NP} + 1$ $B_N \rightarrow B_N + 1$
47	$B_N \rightarrow$	$w_{47} = k_{dn}B_N$	$B_{NP} \rightarrow B_{NP} - 1$ $B_N \rightarrow B_N - 1$
$\frac{dB_{NP}}{dt}$			
48	$B_{NP} \rightarrow$	$w_{48} = (V_{dBN}\Omega)\frac{B_{NP}}{(K_d\Omega) + B_{NP}}$	$B_{NP} \rightarrow B_{NP} - 1$
49	$B_{NP} \rightarrow$	$w_{49} = k_{dn}B_{NP}$	$B_{NP} \rightarrow B_{NP} - 1$
$\frac{dI_N}{dt}$			
50	$I_N \rightarrow$	$w_{50} = (V_{dIN}\Omega)\frac{I_N}{(K_d\Omega) + I_N}$	$I_N \rightarrow I_N - 1$
51	$I_N \rightarrow$	$w_{51} = k_{dn}I_N$	$I_N \rightarrow I_N - 1$
$\frac{dCB^*}{dt}$			
52	$CB^* \rightarrow$	$w_{52} = \Omega\left(\frac{\nu_P}{CB_T}\right)\left[\left(\frac{\nu_K}{\nu_P}\right)\frac{\Omega - CB^*}{K_1 + (\Omega - CB^*)}\right]$	$CB^* \rightarrow CB^* + 1$
53	$CB^* \rightarrow$	$w_{53} = \Omega\left(\frac{\nu_P}{CB_T}\right)\frac{CB^*}{K_2 + CB^*}$	$CB^* \rightarrow CB^* - 1$

Table S4. Model parameter values

Parameter	Value
$k_1(1/h)$	0.4
$k_2(1/h)$	0.2
$k_3(1/(nM \cdot h))$	0.4
$k_4(1/h)$	0.2
$k_5(1/h)$	0.4
$k_6(1/h)$	0.4
$k_7(1/(nM \cdot h))$	0.5
$k_8(1/h)$	0.1
$k_{AP}(nM)$	0.7
$k_{AC}(nM)$	0.6
$k_{IB}(nM)$	2.2
$k_{dmb}(1/h)$	0.01
$k_{dmc}(1/h)$	0.01
$k_{dmp}(1/h)$	0.01
$k_{dn}(1/h)$	0.01
$k_{dnc}(1/h)$	0.12
$K_d(nM)$	0.3
$K_{dp}(nM)$	0.1
$K_p(nM)$	0.1
$K_{mB}(nM)$	0.4
$K_{mC}(nM)$	0.4
$K_{mP}(nM)$	0.31
$k_{sB}(1/h)$	0.12
$k_{sC}(1/h)$	1.6
$k_{sP}(1/h)$	0.6
m	2
n	4
$V_{1B}(nM/h)$	0.5
$V_{1C}(nM/h)$	0.6
$V_{1P}(nM/h)$	0.4
$V_{1PC}(nM/h)$	0.4

Table S4. Cont.

Parameter	Value
$V_{2B}(nM/h)$	0.1
$V_{2C}(nM/h)$	0.1
$V_{2P}(nM/h)$	0.3
$V_{2PC}(nM/h)$	0.1
$V_{3B}(nM/h)$	0.5
$V_{3PC}(nM/h)$	0.4
$V_{4B}(nM/h)$	0.2
$V_{4PC}(nM/h)$	0.1
$V_{phos}(nM/h)$	0.4
$\nu_{dBC}(nM/h)$	0.5
$\nu_{dBN}(nM/h)$	0.6
$\nu_{dCC}(nM/h)$	0.7
$\nu_{dIN}(nM/h)$	0.8
$\nu_{dPC}(nM/h)$	0.7
$\nu_{dPCC}(nM/h)$	0.7
$\nu_{dPCN}(nM/h)$	0.7
$\nu_{mB}(nM/h)$	0.8
$\nu_{mC}(nM/h)$	1.0
$\nu_{mP}(nM/h)$	1.1
$\nu_{sB}(nM/h)$	1.0
$\nu_{sC}(nM/h)$	1.1
$\nu_{sP0}(nM/h)$	1.1
Ω	90
a	10.0
b	4.0
N	49
$K_D(nM)$	2.0
$k(1/h)$	10.0
$\nu_0(nM/h)$	0.5
$\nu_1(nM/h)$	5.0
$V_{MK}(nM/h)$	8.0
$K_a(nM)$	2.5
$CB_T(nM)$	1.0
$K_C(nM)$	0.3
$C_T(nM)$	0.4